RESEARCH ARTICLE | FEBRUARY 23 2026

Continuum modeling of radiation-induced degradation in superconductors FREE

Ihina Mahajan ; Shoham Sen ; Venkat Selvamanickam ; Liping Liu ; Pradeep Sharma

J. Appl. Phys. 139, 085901 (2026)
https://doi.org/10.1063/5.0319382
CHORUS

Journal of Applied Physics ARTICLE pubs.aip.org/aip/jap

Continuum modeling of radiation-induced degradation in superconductors

Cite as: J. Appl. Phys. **139**, 085901 (2026); doi: 10.1063/5.0319382
Submitted: 23 December 2025 · Accepted: 30 January 2026 ·
Published Online: 23 February 2026

Ihina Mahajan,[1] Shoham Sen,[2] Venkat Selvamanickam,[3] Liping Liu,[4,a)] and Pradeep Sharma[5,a)]

AFFILIATIONS

[1]Materials Science and Engineering Program, University of Houston, Houston, Texas 77204, USA
[2]Department of Mechanical Engineering, University of Houston, Houston, Texas 77204, USA
[3]Department of Mechanical Engineering, Advanced Manufacturing Institute, Texas Center for Superconductivity, University of Houston, Houston, Texas 77204, USA
[4]Department of Mathematics, Rutgers University, New Brunswick, New Jersey 08854, USA
[5]Department of Mechanical Engineering, Department of Physics, and the Materials Science and Engineering Program, University of Houston, Houston, Texas 77204, USA

[a)]**Authors to whom correspondence should be addressed:** liu.liping@rutgers.edu and psharma@central.uh.edu

ABSTRACT

Realizing the promise of nuclear fusion requires confining plasma at millions of degrees, a feat achievable only through high-field superconducting magnets. However, the fusion reaction itself generates a relentless flux of high-energy neutrons that degrades these critical and prohibitively expensive coils, limiting the operational lifetime of the reactor and compromising its economic viability. While radiation damage is well-documented experimentally, a predictive theoretical framework that links microscale defects to macroscopic magnetic failure has remained elusive. Here, we bridge this gap with a homogenized continuum damage model based on Ginzburg–Landau theory. By treating radiation-induced defects as "quantized" normal-phase inclusions, we map the degradation of the superconducting order parameter to an equivalent homogenization problem. This approach yields closed-form analytical expressions for the critical current as a function of neutron fluence, magnetic field, and temperature. We calibrate and validate the model against experimental data in the literature on rare-earth barium copper oxide (REBCO) tapes, demonstrating that the complex evolution of superconducting properties, including the counterintuitive "peak effect", can be captured by a few effective material parameters that need to be calibrated just once. This work provides a design tool for engineering radiation-tolerant magnets, a critical step toward sustainable fusion energy.

I. INTRODUCTION

The realization of controlled nuclear fusion relies fundamentally on the magnetic confinement of high-temperature plasma, a process requiring magnetic field strengths that exceed the capabilities of conventional resistive magnets. Consequently, high-field superconducting coils are the critical enabling technology for modern tokamak designs, offering the necessary current density without the prohibitive resistive losses associated with copper conductors. The economic and technical viability of a fusion reactor is, therefore, inextricably linked to the performance and longevity of its superconducting architecture.[1,2] However, the operational environment within a deuterium–tritium fusion reactor is exceptionally hostile. The fusion reaction generates a significant flux of high-energy neutrons as an intrinsic by-product. While reactor designs incorporate radiation shielding, the strict geometric constraints required to maintain a compact, technically feasible tokamak design limit the thickness of this shielding.[3] As a result, a non-negligible fraction of the neutron flux inevitably penetrates to the superconducting coils, subjecting the material to continuous irradiation over its operational lifetime.

The interaction of these high-energy neutrons with the superconductor is destructive. Neutrons collide with the atomic lattice, generating collision cascades that displace atoms and introduce permanent defects into the microstructure. Phenomenologically, this damage manifests as a local suppression of the superconducting transition temperature, T_c. When the local T_c drops below the

operating temperature, these damaged regions undergo a phase transition to the normal (non-superconducting) state. These localized normal zones act as resistive inclusions within the superconducting matrix, effectively reducing the volume available for supercurrent transport. The accumulation of these defects leads to subsequent degradation of the magnet's critical current (I_c) and, by extension, the overall operational lifetime of the reactor. Therefore, developing a robust continuum framework to model and predict this radiation-induced degradation is essential for ensuring the reliability of future fusion power plants.

The theoretical limits of critical current in pristine superconductors are well-established within the Ginzburg–Landau framework.[4,5] However, for technically relevant type-II superconductors, the macroscopic electromagnetic behavior is governed by vortex dynamics. While vortices move freely in an ideal lattice, causing dissipation, microstructural defects act as pinning centers that immobilize them, thereby sustaining a supercurrent. This phenomenon of vortex pinning has been extensively analyzed by incorporating impurities directly into the Ginzburg–Landau equations.[6–11] Subsequent studies have leveraged this framework to link specific pinned vortex configurations to the resulting critical current.[12–17] For instance, Sadovskyy *et al.*[13] utilized large-scale simulations to determine how the specific shape, size, and distribution of inclusions dictate performance. In contrast to these discrete, computationally intensive approaches, we adopt a method of continuum homogenization. Rather than resolving the stochastic variability of individual defects, we propose a phenomenological model that captures the effective macroscopic response. By averaging over the defect distribution, our framework provides a physically transparent explanation for the degradation of the critical current that quantitatively matches experimental observations.

This work establishes a continuum-level framework to model the degradation of superconducting coils in the neutron-rich environment of fusion reactors. By identifying that high-energy neutrons locally suppress the superconducting transition temperature (T_c), we propose a homogenized model wherein discrete damaged regions are treated as normal-phase inclusions within a superconducting matrix. We introduce a "quantized damage" approach that treats stochastic damage events as a cumulative loss of superconducting volume, which allows us to reformulate the Maxwell–London equations into a mathematically tractable linearized problem. This analogy enables the derivation of closed-form analytical expressions for the degradation of critical current (I_c) as a function of damage volume fraction and geometry.

Crucially, our model goes beyond simple monotonic decay. By integrating a phenomenological correction for vortex pinning, we successfully capture the non-monotonic "peak effect," an initial enhancement of I_c observed in experiments at low defect densities. This framework, thus, offers a physically grounded yet computationally efficient tool for predicting magnet lifetime, requiring only a one-time calibration of effective material parameters to guide the design of radiation-tolerant components for future fusion applications.

The remainder of the paper is organized as follows. Section II establishes the theoretical framework, detailing our approach and the failure criterion used to determine the critical current. This section also introduces the "quantized damage model" (Subsection II A), which provides the physical justification for the effective inclusion geometries used in our analysis. Section III applies this framework to derive analytical solutions for the critical current ratio. This derivation is further refined in Subsection III A to account for vortex-induced pinning effects, where we also introduce the damage growth model. Section IV validates these theoretical predictions against experimental data from Fischer *et al.*[18] We first calibrate the material parameters at fixed fields (Subsection IV A) and subsequently analyze their temperature and magnetic field dependence (Subsection IV B). Finally, Sec. V provides concluding remarks. Detailed mathematical derivations are relegated to the Appendix (A, B, C & D) to maintain the flow of the main text.

II. DESCRIPTION OF THE MODEL

In this section, we delineate the theoretical framework for our damage model. To ensure the model remains computationally tractable for engineering applications, we introduce a set of simplifying assumptions. Fundamentally, current flow in a superconductor is non-resistive and reversible; it is governed not by an electric field, but by the magnetic vector potential.[19,20] Consequently, the system can be described within the standard Ginzburg–Landau formalism, which couples the superconducting order parameter (representing the Cooper-pair density) to the magnetic field. The Ginzburg–Landau framework consists of two coupled differential equations: the Ginzburg–Landau equation for the order parameter and Maxwell's equations (specifically Ampère's law) for the current. For simplicity, we assume that the magnitude of the order parameter is spatially uniform within the superconducting domain. This approximation is appropriate in the regime where the penetration depth λ exceeds the characteristic spacing between damage cores. See Appendix A for a more detailed justification.

This assumption decouples the system, allowing us to work primarily with Maxwell's equations. Crucially, we demonstrate that under these conditions, the equations governing supercurrent can be mathematically reformulated as a harmonic flow problem. The detailed derivation of this equivalence is provided in Appendix A. To formulate the mathematical model, we begin with a superconducting domain Ω containing a damaged inclusion denoted by Ω_d. The supercurrent velocity $\boldsymbol{v}:\Omega\backslash\Omega_d \to \mathbb{R}^3$ is defined as non-zero only outside the damaged region. The governing equations for $\boldsymbol{v}$ are given by

$$\begin{aligned} \Delta \boldsymbol{v} &= 0 \text{ in } \Omega\backslash\Omega_d, \\ \operatorname{div} \boldsymbol{v} &= 0 \text{ in } \Omega\backslash\Omega_d, \\ \boldsymbol{v} &= 0 \text{ on } \partial\Omega_d, \\ \boldsymbol{v} &= \boldsymbol{v}_\infty \text{ on } \partial\Omega, \end{aligned} \tag{1}$$

where the boundary condition $\boldsymbol{v} = \boldsymbol{v}_\infty$ on $\partial\Omega$ prescribes the supercurrent velocity on the exterior boundary of the superconductor.

The supercurrent density within the Ginzburg–Landau framework is defined as $\boldsymbol{j} = u^2\boldsymbol{v}$. u^2 in the Ginzburg–Landau theory represents the density of Cooper pairs. Here, the expression for $\boldsymbol{j}$ represents the non-dimensionalized expression for the supercurrent. In a pristine superconductor, the theoretical maximum critical

current density is $j_{\max} = \frac{2}{3\sqrt{3}}$;[5] a detailed derivation of this limit is provided in Appendix B. We adopt this threshold as the local failure criterion for the damaged material: if the magnitude of the current density at any point within the domain exceeds $j_{\max}$, local superconductivity is considered lost. Consequently, the full supercurrent distribution is obtained by first solving for the velocity field $\boldsymbol{v}$ using (1) and subsequently determining the order parameter u via the Ginzburg–Landau energy functional. Provided the local current density remains everywhere below $j_{\max}$, the system maintains its superconducting state. The total macroscopic current is then computed by integrating the local current density over the superconducting domain,

$$I = \int_{\Omega \setminus \Omega_d} j dA. \tag{2}$$

Our primary objective is to determine the critical current, I_c, defined as the total current at the onset of failure—specifically, when $\max_{\Omega \setminus \Omega_d} j = j_{\max}$. Naturally, I_c degrades as the volume fraction of damaged regions increases. Experimental studies, such as those by Fischer *et al.*,[18] quantify this degradation by reporting the ratio I_c/I_c^0 as a function of neutron fluence, where I_c^0 represents the critical current of the pristine superconductor. To bridge our model with these experimental results, we posit a power-law relationship between the neutron fluence and the damaged volume fraction. As the damage volume fraction grows, the probability of a neutron impinging on the superconducting region decreases, as the probability of impinging on the damaged region increases. This implies that the growth of the volume fraction decreases. This tension is captured by a power-law behavior with an exponent less than unity.

It is important to note that the boundary velocity $\boldsymbol{v}_\infty$ in (1) is not a directly observable quantity; rather, the total current I in (2) is the physically measured control parameter. Consequently, determining the state of the system requires using I to solve the inverse problem for $\boldsymbol{v}_\infty$, rendering the determination of $\boldsymbol{j}$ a nonlinear process. To mitigate this complexity, we focus on simple geometries where closed-form solutions for $\boldsymbol{v}$ can be derived.

While the continuum formulation above constitutes the core theoretical contribution of this work, interpreting the physical evolution of damage requires a heuristic framework. In Sec. II A, we introduce the "Quantized Damage Model." This conceptual model provides physical insight into the damage process, motivates the choice of inclusion geometries, and guides the selection of material parameters for fitting experimental data.

A. Quantized damage model

Our proposed model of damage in superconducting coils may be viewed through the lens of a homogenization approach: a discrete, quantized picture of damage induced by neutron impact, followed by a homogenized representation appropriate at macroscopic scales. Each incident neutron locally suppresses superconductivity, creating a damaged zone in the normal phase that obstructs supercurrent flow. Given the stochastic nature of neutron damage, we conceptualize these regions as discrete "quanta." We emphasize that this quantization is a heuristic construct, serving as the basis for homogenization into an effective inclusion embedded within the domain. The flow problem (1) is then applied to this effective inclusion.

The primary advantage of this approach is that the effective damaged region aggregates both normal regions and vortices. Consequently, determining the exact spatial distribution of individual vortices becomes unnecessary.

During the initial stages of the damage process, the volume fraction is small and damaged regions are spatially isolated. The effective problem is, therefore, modeled as a spherical inclusion in a finite domain [see Fig. 1(a)]. As damage accumulates and the distance between regions decreases, the effective inclusion is better approximated as cylindrical [see Fig. 1(b)]. In Sec. III, we employ these geometric assumptions to facilitate closed-form solutions.

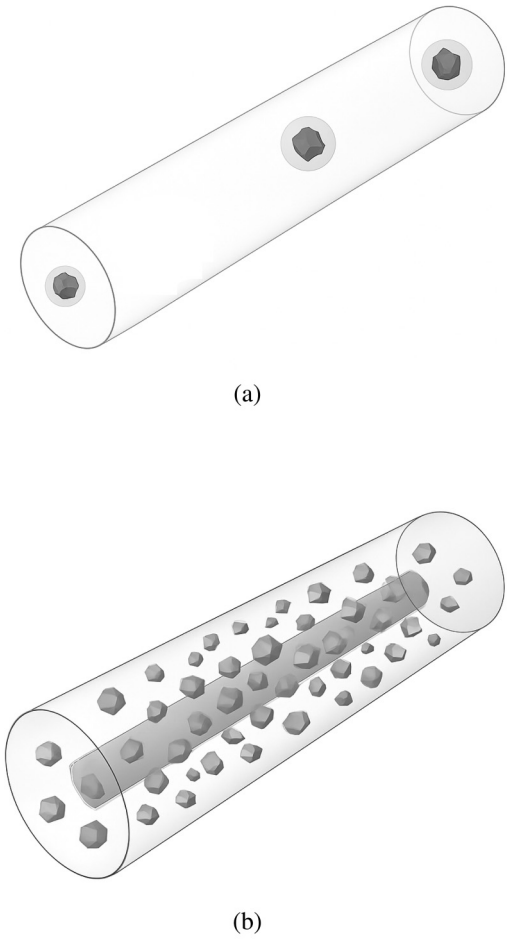

(a)

(b)

FIG. 1. The homogenization of damaged regions to obtain an effective cylindrical inclusion: (a) represents a sparse distribution where individual spheres are homogenized, and (b) represents a dense distribution where the actual damaged regions (solid gray) are represented by a single translucent effective cylinder.

III. THEORETICAL FORMULATION

In this section, we derive solutions to the boundary value problems defined by the formulation in (1). As established previously, the order parameter is determined by minimizing the Ginzburg–Landau energy functional over spatially uniform order parameters, u. For the specific case of zero external magnetic field ($\boldsymbol{H} = 0$), the energy functional is given by

$$G[u, \boldsymbol{v}] = \int_\Omega \frac{(1-u^2)^2}{2} + \frac{\nabla u^2}{\kappa^2} + \boldsymbol{v}^2 u^2 + |\mathrm{curl}\boldsymbol{A}|^2. \tag{3}$$

The derivation of the above form of the energy from the traditional formulation is present in Appendix C. The minimizer of the above can be shown to satisfy

$$u^2 = 1 - \langle \boldsymbol{v}^2 \rangle. \tag{4}$$

The current density is then given as

$$\boldsymbol{j} = u^2 \boldsymbol{v} = (1 - \langle \boldsymbol{v}^2 \rangle)\boldsymbol{v}. \tag{5}$$

Motivated by the quantized damage framework, we consider two effective inclusion geometries: spherical and cylindrical. Although commercial superconductors are typically fabricated as tapes (thin films), we simplify the boundary value problems to ensure analytic tractability. We, therefore, model the system as either (1) a spherical inclusion in an infinite domain or (2) a cylindrical inclusion in a finite cylindrical domain.

Analysis of the spherical case reveals that the total current is independent of the inclusion radius. This leads to the unphysical result that damage has no impact on the critical current, highlighting the limitation of the infinite domain approximation for this geometry. Consequently, we focus our analysis on the cylindrical inclusion within a finite cylindrical domain. Since the primary quantity of interest is the normalized critical current ratio, I_c/I_c^0, the geometric factors associated with the outer domain appear in both the numerator and denominator and, to a first approximation, cancel out.

Consider a cylindrical damaged region of radius R, while the superconducting domain is a cylinder of radius R_1. We define the damaged region volume fraction ϕ as the fraction of the cross-sectional area occupied by the inclusion,

$$\phi = \left(\frac{R}{R_1}\right)^2. \tag{6}$$

This non-dimensional parameter $\phi \in [0, 1]$ serves as a control variable for the extent of degradation due to neutron fluence. Owing to the symmetry of the problem, the velocity in (1) can only depend on r. Rewriting (1) for this case,

$$\frac{1}{r}\frac{\partial}{\partial r}\left(r\frac{\partial v_\theta}{\partial r}\right) - \frac{v_\theta}{r^2} = 0, \quad \frac{1}{r}\frac{\partial}{\partial r}\left(r\frac{\partial v_z}{\partial r}\right) = 0, \quad \frac{1}{r}\frac{\partial}{\partial r}(r v_r) = 0, \qquad \boldsymbol{v}(R) = 0, \quad \boldsymbol{v}(R_1) = v_\infty \hat{e}_z. \tag{7}$$

Notice that the following velocity distribution for the axial velocity satisfies the above equations:

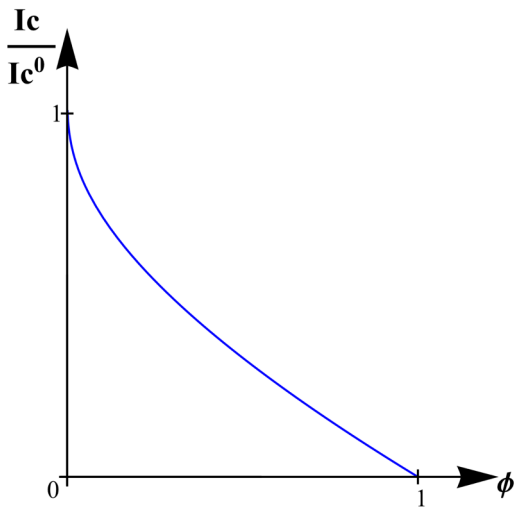

FIG. 2. Normalized critical current $\frac{I_c}{I_c^0}$ as a function of damaged volume fraction ϕ. The plot shows a monotonic decrease, reflecting the progressive loss of superconductivity with increasing damage.

$$v_r = 0, \quad v_\theta = 0, \quad v_z = v_\infty \frac{\log(r/R)}{\log(R_1/R)}. \tag{8}$$

Given $\boldsymbol{v}$, the order parameter can be calculated using (4). We use (5) to compute the total current by integrating $j(r)$ over the undamaged area, from $r = R$ to $r = R_1$. This gives the critical current of the system as

$$I = \int_R^{R_1} j(r)\, dA = u^2 v_\infty \int_R^{R_1} \frac{\log(r/R)}{\log(R_1/R)}\, dA = u^2 v_\infty \pi R_1^2 \left[\frac{1 - \phi + \log\phi}{\log\phi}\right]. \tag{9}$$

Our criterion for failure was that the maximum local current density was equal to $j_{\max} = \frac{2}{3\sqrt{3}}$. Notice that v_z is maximum on the surface of the superconductor. Therefore, failure must occur there. This means that $u^2 v_\infty = j_{\max}$. The total critical current in a pristine superconductor would be $I_c^0 = u^2 v_\infty \pi R_1^2$. Rewriting (9),

$$\frac{I_c}{I_c^0} = \frac{1 - \phi + \log\phi}{\log\phi}, \tag{10}$$

where I_c is the total critical current in the superconductor with damaged region volume fraction ϕ. Figure 2 shows the plot for the critical current ratio in (10).

A. Modification due to vortices

To match the critical current ratio to experimental results, we use the results of Fisher *et al.*[18] We define a relation between the

volume fraction and the fluence of the neutron irradiation as

$$\phi = d\left(\frac{fl}{fl_0}\right)^n = \left(\frac{d}{fl_0^n}\right)fl^n, \tag{11}$$

where, d , fl_0, and n are the material parameters, while fl is the fluence. The above model corresponds to a typical power-law growth model. The constant fl_0 is used to non-dimensionalize the fluence and scale the input. It should be clear from the second relation that the constant of interest is d/fl_0^n. Here, n is a measure of the growth rate of the damage region with the fluence. Specifically, if one draws a log–log plot of the damage volume fraction and the fluence, then n is the slope of the plot. Finally, d is a measure of the damaged volume fraction produced by a single displacement cascade.

If we substitute (11) for (10), then we can compare the results with experiments. We use results from Ref. 18 to produce a schematic for the critical current ratio in Fig. 3. Notice that the relation (11) is monotone. This means that on substituting into (10), we would roughly obtain Fig. 2 (non-uniformly scaled). Comparing Fig. 2 with Fig. 3 shows us that our result does not capture the initial increase at low fluence. According to the discussion in Ref. 18, this increase is due to flux pinning. They established this by introducing artificial pinning centers and observing failure at lower fluence values. In Fischer *et al.*,[18] failure is defined as the point when I_c/I_c^0 goes below 1.

We attribute this discrepancy to the limitations of the uniform order parameter assumption. While a rigorous treatment would require solving the fully coupled Ginzburg–Landau equations to resolve the spatial variation of u, we adopt a phenomenological alternative: accounting for these microstructural effects by modifying the macroscopic failure criterion.

As established in the quantized damage framework, neutron irradiation induces defects that act as pinning centers for magnetic vortices. Physically, each pinned vortex consists of a normal core surrounded by circulating supercurrents that screen the magnetic flux. These local circulating currents superimpose onto the macroscopic transport current. A standard homogenization approach, which treats defects merely as passive voids, neglects this interaction and the resulting enhancement of the current-carrying capacity. To incorporate this effect without abandoning the homogenized framework, we modify the failure criterion. We redefine the critical current density as $j_c = j_{\max}(1 + g(\phi))$, where the term $g(\phi)$ phenomenologically captures the enhancement of the critical current due to vortex pinning as the damaged volume fraction increases.

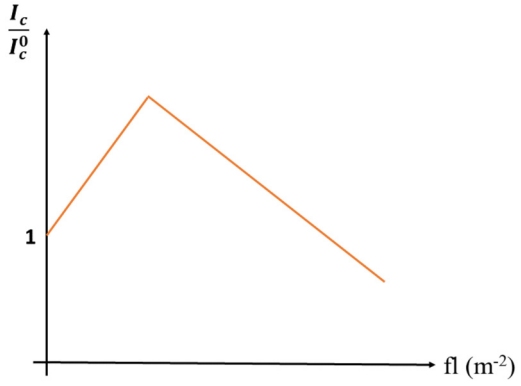

FIG. 3. Schematic trend of the critical current ratio I_c/I_c^0 as a function of neutron fluence, adapted from experiments.[18]

Applying this modified failure criterion to the derivation in Sec. III yields the corrected expression for the critical current ratio,

$$\frac{I_c}{I_c^0} = \frac{(1 - \phi + \log(\phi))}{\log(\phi)}(1 + g(\phi)). \tag{12}$$

The simplest model for $g(\phi)$ is to consider it to be linear. One may even treat it as a linear approximation. Choosing $g(\phi) = c\phi$ gives us

$$\frac{I_c}{I_c^0} = \left(1 + \frac{1 - \phi}{\log\phi}\right)(1 + g(\phi)) = \left(1 + \frac{1 - \phi}{\log\phi}\right)(1 + c\phi). \tag{13}$$

While this has the correct trend for ϕ away from zero (increase followed by decrease), very close to $\phi = 0$, there is a sharp decrease. This initial decrease is due to the log in the denominator in (13). The logarithmic function will dominate any polynomial function, and if one thinks of polynomial expansions for $g(\phi)$, this sharp initial decrease will always remain.

We attribute the sharp unphysical decrease near $\phi \to 0$ to the logarithmic singularity inherent in the 2D cylindrical solution. Since the pinning function $g(\phi)$ is modeled as a polynomial, it is mathematically incapable of counteracting the dominant logarithmic decay in this limit. However, this logarithmic dependence is strictly an artifact of the cylindrical geometry assumption. The fundamental solution (Green's function) for the Laplacian in 2D is logarithmic, whereas in 3D, it decays algebraically. As discussed in the quantized damage model, the low-damage regime ($\phi \ll 1$) consists of sparse, isolated defects that are physically better approximated by spherical inclusions in a finite domain. In this 3D regime, the perturbation to the flow decays as an inverse polynomial, which does not exhibit the singular behavior of the 2D logarithm. Consequently, we treat the logarithmic dominance at low fluence as a geometric limitation of the cylindrical model. We now proceed to show that the critical current ratio depends directly on the average velocity distribution, $I_c/I_c^0 = \langle v \rangle$. The proof is presented below:

$$\begin{aligned} \boldsymbol{v} &= v_\infty \boldsymbol{f}, \\ \boldsymbol{j} &= \boldsymbol{v}u^2 = v_\infty u^2 \boldsymbol{f}, \\ I_c &= |\Omega| v_\infty u^2 \langle \boldsymbol{f} \rangle, \\ \tfrac{I_c}{I_c^0} &= \langle \boldsymbol{f} \rangle, \end{aligned} \tag{14}$$

where we used $|\Omega| v_\infty u^2 = I_c^0$. Further note that we have separated the velocity distribution into a constant component v_∞ and a functional component ($\boldsymbol{f}$). We have assumed a local failure criterion ($u^2 \max_\Omega v < j_c$) and that failure is happening at the surface of the

cylinder where $\boldsymbol{v} = v_\infty \boldsymbol{e}_z$. Since $\boldsymbol{f}$ is harmonic by (1) and $\boldsymbol{f}(\partial\Omega_d) = 0$, the maximum must happen on $\partial\Omega \backslash \partial\Omega_d$.

It is interesting to notice that most solutions of exterior problems (that is what we expect for small inclusions) tend to have a singularity at the origin. The singularity for 2D geometries turns out to be logarithmic. However, for 3D geometries, it is usually inverse polynomials. We, therefore, expect that if we have spherical inclusions, then we can obtain $1/r$ decay of an inverse polynomial in ϕ for $\langle \boldsymbol{f} \rangle$. In this case, a polynomial behavior of g in (13) can be used to avoid the initial decrease associated with the logarithmic solution. However, further away from $\phi \sim 0$, we can treat it like a cylinder for the effective medium. Our result matches experiments in this region.

IV. MATCHING WITH EXPERIMENTAL RESULTS

In this section, we utilize the derived relations (13) and (11) to quantitatively validate our model against the experimental data provided by Fischer *et al.* (see Fig. 6 in Ref. 18). Acknowledging that the effective material parameters are sensitive to environmental conditions, we further analyze the I_c vs H data at 40 and 50 K (Fig. 9 in Ref. 18) to characterize their dependence on temperature and magnetic field. The analysis is structured as follows: Section IV A determines the baseline material parameters for various superconductors under fixed field conditions. Section IV B extends this analysis to a specific representative material—SCS4050 AP 2013 (GdBCO)—to map the evolution of these constitutive parameters across a broad spectrum of temperatures and magnetic fields. This results in a comprehensive closed-form expression for the critical current, enabling predictive modeling over a wide range of operational regimes.

A. Material parameters for a fixed field

In this section, we calibrate the constitutive parameters of our model by fitting (11) and (13) to the experimental data reported by Fischer *et al.* (Fig. 6 in Fischer *et al.*[18]). The experimental dataset encompasses three superconductor types: YBCO tape, GdBCO tape, and GdBCO tape enhanced with artificial pinning centers (designated with the suffix "AP"). Consistent with our homogenized framework, we conceptualize these artificial pinning centers as a field of pre-existing damage.

We introduce a fluence scaling constant, $fl_0 = 7$, determined through empirical optimization. A key finding of Fischer *et al.* was that while pinning centers initially enhance critical current, they accelerate the degradation process, leading to earlier failure.[21] They attributed this to the fact that radiation damage itself generates pinning centers; thus, samples with artificial pinning centers effectively begin with a non-zero damage accumulation. We incorporate this physical insight by introducing an offset, ε, to the damaged volume fraction,

$$\frac{I_c}{I_c^0} = \left(1 + \frac{1 - (\phi + \varepsilon)}{\log(\phi + \varepsilon)}\right)(1 + c(\phi + \varepsilon)), \tag{15}$$

where ε represents the effective volume fraction of the pre-existing artificial pinning centers.

Furthermore, the exponent n in (11) governs the growth rate of damage as a function of fluence. This rate is fundamentally determined by the interaction between the incident neutron energy spectrum and the lattice. Since the neutron source (and thus the energy spectrum) remains constant across the experiments,[22] the defect production mechanics are consistent. Consequently, we treat n as a parameter characteristic of the radiation source rather than the material. We, therefore, fix n as a universal constant for this dataset, with a fitted value of $n = 0.333\,81$.

This leaves c and d as the primary material-dependent parameters, with ε serving as the specific shift parameter for the SCS4050 AP samples. The best-fit values for these parameters are summarized in Table I (Appendix D). Figure 4 illustrates the correspondence between our theoretical model (15) and the experimental results of Fischer *et al.*,[18] demonstrating a robust fit across all material classes. The quality of the fits shown in Fig. 4 was quantified using the root mean square error (RMSE) between the experimental data points taken from Ref. 18 and the model predictions evaluated at the same fluence values. The RMSE values range from 1.8×10^{-4} to 5.8×10^{-2} across the materials considered. The RMSE values can be found in Table I of Appendix D.

B. SCS4050 AP 2013 material parameter variation with field and temperature

In this section, we extend our analysis to capture the magnetic field and temperature dependence of the critical current, matching the experimental results for SCS4050 AP 2013 presented in Fig. 9 of Fischer *et al.*[18] Recall that the baseline calibration for this material was established at a reference point of 30 K and 15 T (see Table I).

To accurately model the material behavior across the full variations of T and H, we allow the constitutive parameters c and d to

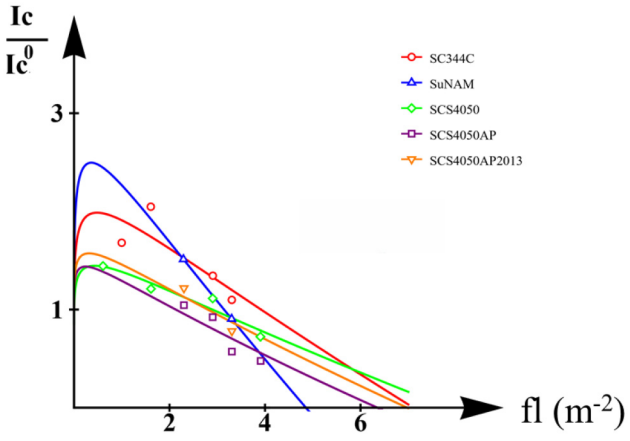

FIG. 4. Normalized critical current as a function fluence for different superconductors. The vertical axis shows the critical current normalized by its pristine (unirradiated) value, I_c/I_c^0, while the horizontal axis represents the fluence *fl*. Symbols denote experimental data taken from Ref. 18 for five materials: SC344C (red circles), SuNAM (blue triangles), SCS4050 (green diamonds), SCS4050AP (purple squares), and SCS4050AP2013 (orange inverted triangles). Solid lines correspond to fits obtained using the theoretical model given in Eq. (13).The fitted parameters can be found in Table I of Appendix D.

evolve. Our fitting procedure indicates that the pinning enhancement parameter, c, is effectively a function of temperature alone, whereas the damage susceptibility parameter, d, depends on both the temperature and the applied magnetic field. The derived empirical relations for $c(T)$ and $d(H, T)$ are plotted in Fig. 5,

$$\begin{aligned} c(T) &= 14.6007 - 0.215\,342T, \\ d(H, T) &= 1.008 - 0.014\,915H + 0.000\,328\,077H^2 \\ &\quad - 0.001\,424\,4T + 0.000\,324\,706\,7HT. \end{aligned} \tag{16}$$

It is important to note that while (16)(a) expresses c solely as a function of temperature, this represents an approximation based on the empirical observation that c is only weakly dependent on the magnetic field H.

Our analysis focuses on the regime where radiation initially enhances the critical current ratio before degradation sets in. We define the failure threshold as the point where this ratio falls below unity. To quantify the material's lifespan under these conditions, we determine the *critical volume fraction* (ϕ^*) and the corresponding *critical fluence* (fl^*) as functions of temperature and magnetic field.

The critical volume fraction is obtained by setting the right-hand side of (13) to unity. Since ϕ^* depends exclusively on c, which in turn depends only on T, we obtain a univariate relationship $\phi^*(T)$ [see Fig. 6(a)]. To derive the physically observable critical fluence $fl^*(H, T)$, we substitute this result into the damage evolution law (11), incorporating the field-dependent parameter $d(H, T)$ [see Fig. 6(b)].

Figure 5(a) indicates that increasing temperature reduces the magnitude of c. Physically, a lower c diminishes the vortex pinning

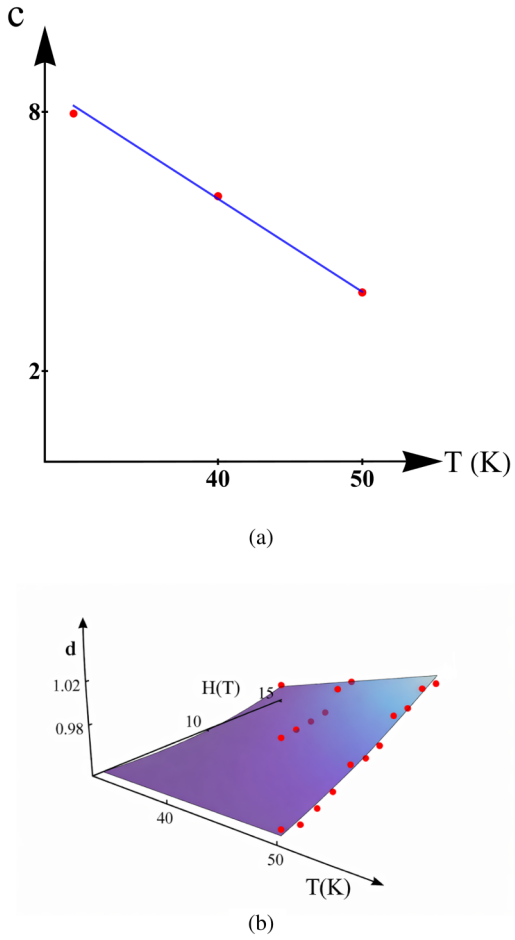

FIG. 5. Temperature and magnetic field dependence of material parameters for SCS4050AP. (a) Parameter c as a function of temperature T. (b) Parameter d as a function of temperature T and magnetic field H. Red dots denote values extracted from experimental data, while solid lines and surfaces represent interpolated trends used in the model.

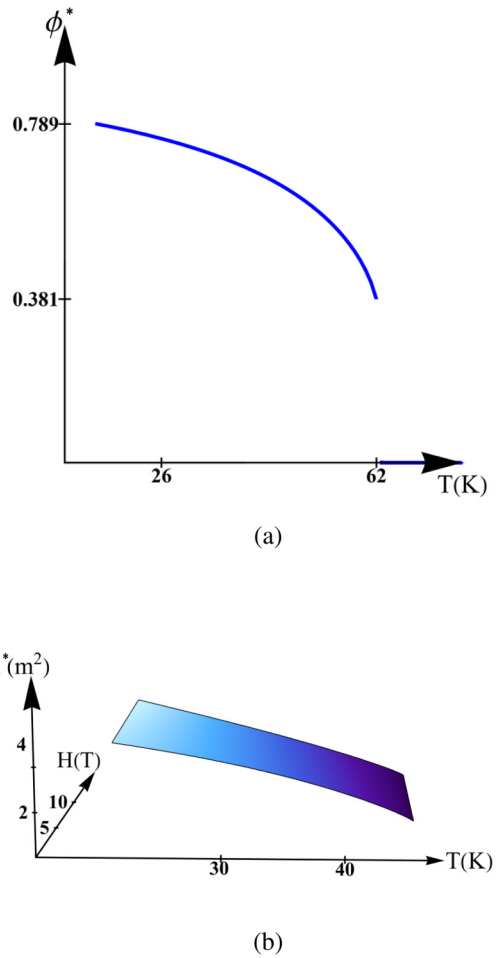

FIG. 6. Temperature and magnetic field dependence of critical parameters for SCS4050. (a) Critical volume fraction ϕ^* as a function of temperature T. (b) Critical fluence fl^* as a function of magnetic field H and temperature T.

contribution to the failure criterion, leading to accelerated degradation. Notably, beyond a critical temperature, the initial enhancement is insufficient to raise the critical current ratio above unity. Mathematically, this corresponds to the disappearance of real solutions of the enhancement condition in the interval $0 < \phi < 1$. Consequently, no damage fraction yields $I_c/I_c^0 > 1$, and the critical volume fraction ϕ^* is set to zero, as shown in Fig. 6(a), reflecting the absence of any physically admissible solution yielding $I_c/I_c^0 > 1$.

Using the derived $\phi^*(T)$, the critical fluence can be expressed as

$$fl^* = fl_0 \left(\frac{\phi^*(T)}{d(H, T)} \right)^{\frac{1}{n}}. \tag{17}$$

A key advantage of (17) is the partial decoupling of dependencies: the failure threshold is determined solely by T (via ϕ^*), while the damage accumulation rate is modulated by both H and T (via d). This structure allows for targeted optimization: by characterizing $c(T)$ and $d(H, T)$, one can identify the specific operating conditions that maximize the critical fluence fl^* [as visualized in Fig. 6(b)].

V. CONCLUDING REMARKS

The durability of superconducting magnets under high-energy neutron irradiation remains one of the definitive engineering challenges for sustained nuclear fusion. In this work, we address this issue by establishing a homogenized continuum framework that maps stochastic microscale damage to a predictable macroscopic response. By mapping the suppression of the superconducting order parameter to a homogenization problem, we provide a physically grounded model that yields closed-form analytical solutions, circumventing the need for computationally expensive (and intractable at the required scale) atomistic simulations.

Our results demonstrate that the complex evolution of the critical current, including the counter-intuitive initial enhancement due to flux pinning, can be captured by a compact set of effective material damage parameters. We have validated this approach against experimental data for rare-earth barium copper oxide (REBCO) tapes and explicitly mapped the degradation limits for SCS4050, offering a quantitative prediction of its operational lifespan under reactor conditions. Ultimately, this framework serves as a bridge between fundamental radiation physics and practical magnet engineering, providing a robust design tool to optimize the reliability and longevity of future fusion confinement systems.

ACKNOWLEDGMENTS

P.S. acknowledges the support of the NSF grant (No. 2437028) and the Cullen Chair from the University of Houston. L.L. acknowledges the NSF grant (No. 2437029).

AUTHOR DECLARATIONS

Conflict of Interest

The authors have no conflicts to disclose.

Author Contributions

Ihina Mahajan: Conceptualization (lead); Formal analysis (equal); Funding acquisition (equal); Investigation (equal); Methodology (equal); Project administration (equal); Resources (equal); Supervision (equal); Validation (equal); Visualization (equal); Writing – original draft (equal); Writing – review & editing (equal). **Shoham Sen:** Formal analysis (lead); Methodology (lead); Visualization (lead); Writing – original draft (lead). **Venkat Selvamanickam:** Formal analysis (supporting); Writing – review & editing (supporting). **Liping Liu:** Conceptualization (equal); Formal analysis (equal); Funding acquisition (equal); Methodology (equal); Project administration (equal); Resources (supporting); Supervision (equal); Writing – original draft (supporting); Writing – review & editing (supporting). **Pradeep Sharma:** Conceptualization (lead); Formal analysis (supporting); Funding acquisition (equal); Investigation (equal); Methodology (equal); Project administration (equal); Resources (equal); Supervision (equal); Validation (equal); Visualization (equal); Writing – original draft (supporting); Writing – review & editing (supporting).

DATA AVAILABILITY

The data that support the findings of this study are available within the article.

APPENDIX A: DERIVATION OF A FLOW PROBLEM

Our starting point is the non-dimensionalized Ginzburg–Landau Energy. The reader is encouraged to visit Appendix C for the derivation. We present the functional here for convenience,

$$G[u, \boldsymbol{v}, \boldsymbol{A}] = \int_{\Omega \backslash \Omega_d} \frac{(1-u^2)^2}{2} + u^2 \boldsymbol{v}^2 + |\mathrm{curl}\boldsymbol{A}|^2 \quad \text{subject} \quad \text{to}\, \boldsymbol{v} = \nabla\chi - \boldsymbol{A}. \tag{A1}$$

We choose a test function for the minimizer uniform u in the region that is superconducting and $u = 0$ in the normal region. A transition between them will contribute as surface energy. With this restriction, we can minimize (A1) with respect to $\boldsymbol{v}$ to obtain

$$\begin{aligned} \mathrm{curlcurl}\boldsymbol{v} + u^2\boldsymbol{v} &= 0 \quad \text{in}\, \Omega\backslash\Omega_d, \\ \boldsymbol{v} &= 0 \quad \text{in}\, \Omega_d, \end{aligned} \tag{A2}$$

where Ω_d is the damaged region and the domain is Ω. Notice that the above implies

$$\mathrm{div}\ \boldsymbol{v} = 0 \quad \text{in}\, \Omega\backslash\Omega_d. \tag{A3}$$

Therefore, Eq. (A2) may be rewritten as $\Delta\boldsymbol{v} = u^2\boldsymbol{v}$. We focus on the regime in which the characteristic spacing between damage cores, denoted by d, is small compared to unity. In dimensional terms, this corresponds to the penetration depth λ being larger than the typical inter-damage-core distance. For superconductors, λ is typically of order 0.1--1 μm, while the thickness of superconducting tapes is also of the order of 1 μm, so these length scales are initially comparable. As neutron irradiation increases, the density

of damage cores rises and the average spacing d decreases substantially, eventually becoming much smaller than λ.

Since the vector field $\boldsymbol{v}$ is constrained to vanish inside each damage core, it must vary from zero to a finite value over a distance of order d in the surrounding superconducting region $\Omega \setminus \Omega_d$. Consequently, spatial variations of $\boldsymbol{v}$ occur on the length scale d, implying that $\mathrm{curlcurl}\boldsymbol{v} \sim \boldsymbol{v}/\mathrm{d}^2$. In the regime $d \ll 1$, this term dominates the right-hand side $u^2\boldsymbol{v} = O(1)$ (the super-current transported is order unity). Under these conditions, the term $u^2\boldsymbol{v}$ in Eq. (A2) may be safely neglected.

We are, therefore, led to the following boundary value problem for $\boldsymbol{v}: \Omega \setminus \Omega_d \to \mathbb{R}^3$:

$$\begin{aligned} \Delta \boldsymbol{v} &= 0 \text{ in } \Omega \setminus \Omega_d, \\ \operatorname{div} \boldsymbol{v} &= 0 \text{ in } \Omega \setminus \Omega_d, \\ \boldsymbol{v} &= 0 \text{ on } \partial\Omega_d, \\ \boldsymbol{v} &= \boldsymbol{v}_\infty \text{ on } \partial\Omega. \end{aligned} \tag{A4}$$

APPENDIX B: MAXIMUM CRITICAL CURRENT

In this section of the Appendix, we derive the relation for the maximum critical current. Consider a pristine superconductor with current being driven by some external means. We further assume that there is no external field. The Ginzburg-Landau functional in (3) can be written as

$$\begin{aligned} G[u, \boldsymbol{v}, \boldsymbol{A}] = \int_{\Omega \setminus \Omega_d} \frac{(1-u^2)^2}{2} + u^2\boldsymbol{v}^2 + |\mathrm{curl}\boldsymbol{A}|^2 \\ \text{subject} \quad \text{to } \boldsymbol{v} = \nabla\chi - \boldsymbol{A}, \end{aligned} \tag{B1}$$

where χ is some scalar. To find the equilibrium configuration corresponding to the maximum possible current flowing in the system, we want to minimize the energy associated with the thermodynamic state, which is a superconductor with a supercurrent flowing in it. To minimize the energy, note that we can pick $\boldsymbol{v}$ to be constant. This makes the last term 0. Picking u uniform gets rid of the second term. Thus, uniform functions are minimizers. The minima of the above give us

$$u^2 = 1 - \boldsymbol{v}^2. \tag{B2}$$

The expression for the current is $\boldsymbol{j} = u^2 v$. The current at equilibrium is, therefore, given by $\boldsymbol{j} = (1-\boldsymbol{v}^2)\boldsymbol{v}$. The maximum value of this current is achieved when $|\boldsymbol{v}| = 1/\sqrt{3}$. The critical current is then given by $j_{\max} = \frac{2}{3\sqrt{3}}$.

To test the stability of this state, one can plug in this solution into the energy functional and compute the corresponding energy,

$$G\left[\sqrt{\frac{2}{3}}, \frac{1}{\sqrt{3}}\right] = \frac{5}{18}. \tag{B3}$$

Notice that the energy above is less than $\frac{1}{2}$, which is the energy associated with the normal state ($u = 0$, $\mathrm{curl}\boldsymbol{A} = \mathrm{H}$). This state, with the current flowing through it, is, therefore, thermodynamically stable.

APPENDIX C: NON-DIMENSIONALIZED GINZBURG–LANDAU ENERGY

We start with the Ginzburg–Landau (GL) free energy for a superconductor, neglecting magnetic field effects,

$$\begin{aligned} G[\psi, \boldsymbol{A}; \boldsymbol{H}] = \int_\Omega \frac{\beta}{2}\left(|\psi|^2 + \frac{\alpha}{\beta}\right)^2 + \frac{1}{2m^*}\left|\frac{\hbar}{i}\nabla\psi - \frac{e^*}{c}\boldsymbol{A}\psi\right|^2 \\ + \frac{1}{8\pi}\int_{\mathbb{R}^3} |\mathrm{curl}\boldsymbol{A} - \boldsymbol{H}|^2. \end{aligned} \tag{C1}$$

Now, performing the substitution $\psi = ue^{i\theta}$, we obtain

$$\begin{aligned} G[ue^{i\theta}, \boldsymbol{A}; \boldsymbol{H}] = \int_\Omega \frac{\beta}{2}\left(u^2 \pm \frac{\alpha}{\beta}\right)^2 + \frac{\hbar^2}{2m^*}(\nabla u)^2 \\ + \frac{\hbar^2}{2m^*}u^2\left(\nabla\theta - \frac{e^*}{\hbar c}\boldsymbol{A}\right)^2 + \int_{\mathbb{R}^3} \frac{|\mathrm{curl}\boldsymbol{A} - \boldsymbol{H}|^2}{8\pi} \\ := \tilde{G}[u, \theta, \boldsymbol{A}; \boldsymbol{H}]. \end{aligned} \tag{C2}$$

We now define the supercurrent velocity as $m^*\boldsymbol{v}/\hbar = \nabla\theta - e^*\boldsymbol{A}/\hbar c$. This modifies the energy functional to give us

$$\begin{aligned} \tilde{G}[u, \boldsymbol{v}, \boldsymbol{A}; \boldsymbol{H}] = \int_\Omega \frac{\beta}{2}\left(u^2 + \frac{\alpha}{\beta}\right)^2 + \frac{\hbar^2}{2m^*}(\nabla u)^2 + \frac{m^*}{2}u^2\boldsymbol{v}^2 \\ + \int_{\mathbb{R}^3} \frac{|\mathrm{curl}\boldsymbol{A} - \boldsymbol{H}|^2}{8\pi}. \end{aligned} \tag{C3}$$

The advantage of the above form is that it is gauge invariant. We will now simplify it further by performing the substitution $x' = x/\lambda$ and $u_\infty^2 = |\alpha|/\beta$, where λ is the penetration depth ($\Omega' = \Omega/\lambda$),

$$\begin{aligned} \frac{\tilde{G}[u, \boldsymbol{v}, \boldsymbol{A}; \boldsymbol{H}]}{\frac{\alpha^2}{\beta}\lambda^3} = \int_{\Omega'} \frac{1}{2}\left(\left(\frac{u}{u_\infty}\right)^2 \pm 1\right)^2 \\ + \frac{\hbar^2}{2m^*\alpha\lambda^2}\left(\nabla'\left(\frac{u}{u_\infty}\right)\right)^2 + \frac{m^*}{2\alpha}\left(\frac{u}{u_\infty}\right)^2\boldsymbol{v}^2 \\ + \frac{e^{*2}}{c^2}\frac{1}{2m^*\alpha}\int_{\mathbb{R}^3} |\mathrm{curl}'\boldsymbol{A} - \lambda\boldsymbol{H}|^2, \end{aligned} \tag{C4}$$

where the + sign is supposed to be taken above the transition temperature and the − sign is used below the transition temperature.

We define

$$\begin{aligned}
&\frac{e^*}{c}\frac{1}{\sqrt{2m^*\alpha}}\boldsymbol{A} = \boldsymbol{A}',\\
&\frac{m^*}{\hbar}\xi\boldsymbol{v} = \frac{\nabla'\theta}{\kappa} - \xi\frac{e^*}{\hbar c}\boldsymbol{A},\\
&\sqrt{\frac{m^*}{2\alpha}}\boldsymbol{v} = \frac{\nabla'\theta}{\kappa} - \frac{1}{\sqrt{2m^*\alpha}}\frac{e^*}{c}\boldsymbol{A},\\
&\boldsymbol{v}' = \frac{\nabla'\theta}{\kappa} - \boldsymbol{A}' = \sqrt{\frac{m^*}{2\alpha}}\boldsymbol{v}.
\end{aligned} \tag{C5}$$

We can use this to simplify the expression for the energy above to obtain

$$\begin{aligned}
G'[u', \boldsymbol{v}', \boldsymbol{A}'; \boldsymbol{H}'] := \frac{\alpha^2}{\beta}\lambda^3\Bigg[\int_{\Omega'}\frac{(1 \pm u'^2)^2}{2} + \left(\frac{\nabla' u'}{\kappa}\right)^2\\
+ u'^2\boldsymbol{v}'^2 + \int_{\mathbb{R}^3}|\mathrm{curl}'\boldsymbol{A}' - \boldsymbol{H}'|^2\Bigg],
\end{aligned} \tag{C6}$$

where $u' = u/u_\infty$ and $(\lambda e^*/c\sqrt{2m^*\alpha})\boldsymbol{H} = \boldsymbol{H}'$. Dropping the primes for convenience and assuming $\boldsymbol{H} = 0$, we obtain

$$G[u, \boldsymbol{v}] = \int_\Omega \frac{(1-u^2)^2}{2} + \frac{\nabla u^2}{\kappa^2} + \boldsymbol{v}^2u^2 + |\mathrm{curl}\boldsymbol{A} - \boldsymbol{H}|^2. \tag{C7}$$

APPENDIX D: MATERIAL PARAMETERS FOR A BEST FIT

In this Appendix, we present the material parameters that best fit the experimental data of Fischer *et al.* (Fig. 6), which have been reproduced in Fig. 4. We fit the model (13) to the critical current ratio as a function of fluence in order to determine the material parameters c and d. For the specific superconductor SCS4050, an additional parameter ε is required; see (15) and the corresponding discussion. The resulting material parameters are summarized in Table I.

TABLE I. Material parameters c, d, and ε, and the root mean square error (RMSE) between experimental data and model predictions for the superconductors considered.

Superconductor	c	d	ε	RMSE
344C (YBCO)	11.8861	0.9948	…	1.8×10^{-4}
SuNAM (GdBCO)	15.5512	1.129 59	…	3.9×10^{-2}
SCS4050 (GdBCO)	7.960 71	0.962 967	…	5.8×10^{-2}
SCS4050 AP	10.0569	1.109 48	0.0676	5.5×10^{-3}
SCS4050 AP (2013)	11.5984	1.106 25	0.0380	8.8×10^{-3}

APPENDIX E: RENORMALIZATION OF A DAMAGE PARAMETER DUE TO A FLUENCE SPECTRUM

The neutron fluence is calculated as

$$fl = \int_0^\infty \Phi(E)dE, \tag{E1}$$

where $\Phi(E)$ is the fluence spectrum (neutrons per unit area per unit energy). Neutrons of different energies will not produce the same amount of damage, so we introduce a simple "damage weight" $w(E)$, which is larger where neutrons are more effective at creating defects. We define a damage-weighted fluence or damage dose

$$D = \int_0^\infty w(E)\Phi(E)dE, \tag{E2}$$

where the above represents how high-energy neutrons contribute more to D through a larger $w(E)$.

For a fixed irradiation spectrum (as in Ref. 18), the shape of $\phi(E)$ and the function $w(E)$ are both fixed. Then, the ratio

$$k_{spec} = \frac{D}{fl} = \frac{\int_0^\infty w(E)\Phi(E)dE}{\int_0^\infty \Phi(E)dE} \tag{E3}$$

is a constant that depends only on that spectrum. So, for this experiment, $D = k_{spec}fl$.

We write our physical law for each energy as

$$\phi = d\left(\frac{D}{D_0}\right)^n, \tag{E4}$$

where ϕ is the damaged region volume fraction, D is the damage-weighted fluence, D_0 is a normalizing constant, and n is the growth parameter describing the average number of impinging neutrons on the material. We have assumed here that n is roughly constant for the energies of interest. Using $D = k_{spec}fl$, the above transforms into the familiar form of (11),

$$\phi = d_{eff}\left(\frac{fl}{fl_0}\right)^n. \tag{E5}$$

Notice that even if we have single energy (a delta function as the spectrum), the relation between ϕ and fl remains unchanged.

REFERENCES

[1] J. Freidberg, F. Mangiarotti, and J. Minervini, "Designing a tokamak fusion reactor—How does plasma physics fit in?" Phys. Plasmas **22**, 070901 (2015).

[2] M. Paidpilli, C. Goel, B. Sarangi, S. Chen, E. Galstyan, J. Jaroszynski, G. Bradford, D. Abraimov, and V. Selvamanickam, "40-meter-long REBCO tapes with critical current over 4,000 a/12 mm at 4.2 K and 13 T by advanced MOCVD," Superconductivity **9**, 100081 (2024).

[3] D. Torsello, D. Gambino, L. Gozzelino, A. Trotta, and F. Laviano, "Expected radiation environment and damage for YBCO tapes in compact fusion reactors," Supercond. Sci. Technol. **36**, 014003 (2023).

[4] M. N. Kunchur, S.-I. Lee, and W. N. Kang, "Pair-breaking critical current density of magnesium diboride," Phys. Rev. B **68**, 064516 (2003).

[5]M. Tinkham, *Introduction to Superconductivity* (Courier Corporation, 2004).
[6]D. Dew-Hughes, "Flux pinning mechanisms in type II superconductors," Philos. Mag. **30**, 293–305 (1974).
[7]A. Campbell and J. Evetts, "Flux vortices and transport currents in type II superconductors," Adv. Phys. **21**, 199–428 (1972).
[8]A. Campbell, "Pinning and critical currents in type II superconductors," Jpn. J. Appl. Phys. **26**, 2053 (1987).
[9]A. Aftalion, E. Sandier, and S. Serfaty, "Pinning phenomena in the Ginzburg–Landau model of superconductivity," J. Math. Pures Appl. **80**, 339–372 (2001).
[10]A. Xu, L. Delgado, N. Khatri, Y. Liu, V. Selvamanickam, D. Abraimov, J. Jaroszynski, F. Kametani, and D. Larbalestier, "Strongly enhanced vortex pinning from 4 to 7 K in magnetic fields up to 31 T in 15 mol.% Zr-added (Gd, Y)-Ba-Cu-O superconducting tapes," APL Mater. **2**, 046111 (2014).
[11]G. Majkic, R. Pratap, A. Xu, E. Galstyan, and V. Selvamanickam, "Over 15 MA/cm^2 of critical current density in 4.8 μm thick, Zr-doped (Gd, Y) $Ba_2Cu_3O_x$ superconductor at 30 K, 3 T," Sci. Rep. **8**, 6982 (2018).
[12]M. Miura, G. Tsuchiya, T. Harada, K. Sakuma, H. Kurokawa, N. Sekiya, Y. Kato, R. Yoshida, T. Kato, K. Nakaoka *et al.*, "Thermodynamic approach for enhancing superconducting critical current performance," NPG Asia Mater. **14**, 85 (2022).
[13]I. A. Sadovskyy, A. E. Koshelev, W.-K. Kwok, U. Welp, and A. Glatz, "Targeted evolution of pinning landscapes for large superconducting critical currents," Proc. Natl. Acad. Sci. U.S.A. **116**, 10291–10296 (2019).
[14]I. Sadovskyy, A. Koshelev, C. L. Phillips, D. A. Karpeyev, and A. Glatz, "Stable large-scale solver for Ginzburg–Landau equations for superconductors," J. Comput. Phys. **294**, 639–654 (2015).
[15]A. E. Koshelev, I. A. Sadovskyy, C. L. Phillips, and A. Glatz, "Optimization of vortex pinning by nanoparticles using simulations of the time-dependent Ginzburg-Landau model," Phys. Rev. B **93**, 060508 (2016).
[16]E. Galstyan, R. Pratap, G. Majkic, M. Kochat, D. Abraimov, J. Jaroszynski, and V. Selvamanickam, "In-field critical current and pinning mechanisms at 4.2 K of Zr-added REBCO coated conductors," Supercond. Sci. Technol. **33**, 074007 (2020).
[17]M. H. Gharahcheshmeh, G. Majkic, E. Galstyan, A. Xu, Y. Zhang, X. Li, and V. Selvamanickam, "Control of in-field performance of 25 mol.% Zr-added REBCO superconductor tapes," Phys. C **553**, 26–32 (2018).
[18]D. X. Fischer, R. Prokopec, J. Emhofer, and M. Eisterer, "The effect of fast neutron irradiation on the superconducting properties of REBCO coated conductors with and without artificial pinning centers," Supercond. Sci. Technol. **31**, 044006 (2018).
[19]C. S. Yeh and K. C. Chen, "A phenomenological theory for elastic superconductors," Contin. Mech. Thermodyn. **5**, 127–143 (1993).
[20]C. Yeh and K. Chen, "A variational principle for the macroscopic theory of elastic type-II superconductors," Proc. R. Soc. Lond. Ser. A **454**, 1911–1921 (1998).
[21]Recall that failure is defined as the point where the ratio $1I_cI_c^0$ drops below unity.
[22]We assume a mono-energetic neutron approximation for simplicity. In reality, the source produces a spectrum of energies. However, as detailed in Appendix E, accounting for the full spectrum simply renormalizes the parameter d into an effective source-dependent parameter, without altering the functional form of the power law.